Supplementary material

Section 1. Models and simulations considered in this study

CMIP6 ESM	**ripf piControl**	**ripf historical**	**Land-vegetation model**	**CMIP6 ESM Reference**
ACCESS-ESM1.5	r1i1p1f1	r10i1p1f1	CABLE2.4/CASA-CNP	[49]
CanESM5-CanOE	r1i1p2f1	r3i1p2f1	CLASS3.6/CTEM1.2	[50,51]
CESM2	r1i1p1f1	r11i1p1f1	CLM5	[52]
CESM2-FV2	r1i1p1f1	r3i1p1f1	CLM5	[52]
CESM2-WACCM	r1i1p1f1	r3i1p1f1	CLM5	[52]
CESM2-WACCM-FV2	r1i1p1f1	r3i1p1f1	CLM5	[52]
CMCC-ESM22	r1i1p1f1	r1i1p1f1	CLM4.5	[53]
CNRN-ESM2-1	r1i1p1f2	r10i1p1f2	SURFEXv8.0/ISBA-CTRIP	[54]
INM-CM4-8	r1i1p1f1	r1i1p1f1	INM-LND1	[55]
INM-CM5-0	r1i1p1f1	r10i1p1f1	INM-LND1	[56]
IPSL-CM5A2-INCA	r1i1p1f1	r1i1p1f1	ORCHIDEE	[57]
MIROC-ES2L	r1i1p1f2	r30i1p1f2	MATSIRO6.0+ VISIT-e ver.1.0	[58]
MRI-ESM2	r1i2p1f1	r1i2p1f1	HAL 1.0	[59]
NorESM2-LM	r1i1p1f1	r3i1p1f1	CLM5	[60]
NorESM2-MM	r1i1p1f1	r3i1p1f1	CLM5	[60]
UKESM1-0-LL	r1i1p1f1	r19i1p1f2	JULES-ES-1.0	[61]
MPI-ESM1-2-LR	r2i1p1f1	r30i1p1f1	JSBACH3.20	[62]
IPSL-CM6A-LR	r1i1p1f1	r26i1p1f1	ORCHIDEE v2.0	[63]
EC-Earth3-CC	r1i1p1f1	r4i1p1f1	HTESSEL/LPJ-GUESS	[64]
MPI-ESM-1-2-HAM	r1i1p1f1	r3i1p1f1	JSBACH 3.20	[65]

Table 1.1. List of CMIP6 ESMs for which all the variables used in this study (i.e. SST, 2-meter air temperature, precipitation, nbp, fgco2) are available in ESGF for both historical and piControl

simulations. The models highlighted in bold in the column "CMIP6 ESM" are the models for which *land-hist* simulation data were also available on ESGF.

Section 2: Details of the signal decomposition

To understand the origins of the inter-model differences in $\sigma^2_{t,\frac{dCO2}{dt}}$, $\sigma^2_{t,Land}$ and $\sigma^2_{t,Ocean}$, we use a signal decomposition similar to the one used for Analysis of Variance[66-67] (ANOVA). Here, we start by reminding the general assumptions of an ANOVA decomposition, then we describe how it translates to our specific purposes.

A-a) general ANOVA decomposition:

Let suppose that a generic variable x is available for M different models, T time steps and R different simulation realizations. A given state of x can be designated as x_{mtr}, where m represents the model ($m = 1,..., M$), t the time step (t=1,...,T) and r the number of realizations for each model ($r = 1,..., R$). We can decompose x_{mtr} as:

$$x_{mtr} = \mu + \alpha_m + \beta_t + \varepsilon_{mt} + \gamma_{mtr} \quad \text{(eq. 2.1)}$$

where:

$\mu = \frac{1}{M}\sum_{m=1}^{M}\frac{1}{T}\sum_{t=1}^{T}\frac{1}{R}\sum_{r=1}^{R} x_{mjr}$ represents the multi-model mean state,

$\alpha_m = \frac{1}{T}\sum_{t=1}^{T}\frac{1}{R}\sum_{r=1}^{R}(x_{mtr} - \mu)$ is the deviation of the model m mean state from the multi-model mean state,

$\beta_t = \frac{1}{M}\sum_{m=1}^{M}\frac{1}{R}\sum_{r=1}^{R}(x_{mtr} - \mu)$ is the multi-model mean temporal variations, which in our case represents the multi-model mean response to the time varying external forcings,

$\varepsilon_{mt} = \frac{1}{R}\sum_{r=1}^{R}(x_{mtr} - \alpha_m - \beta_t - \mu)$ is the externally forced response of model m that deviates from the multi-model mean externally forced response, and

$\gamma_{mtr} = x_{mtr} - \varepsilon_{mt} - \alpha_m - \beta_t - \mu$ is the residual term, assumed to represent the pure internal variability of x_{mtr} (also sometimes referred to as the noise), which is used in ANOVA to estimate whether variability in x is consistent or not with variability solely arising from internal variability.

A-b) Specific signal decomposition for our analysis

In the present study, we are focusing on temporal variation differences among models and not in mean states differences. Therefore, we removed to all models their associated mean state. Conceptually, the statistical decomposition we use to analyze *historical* simulations can be described as:

$$x_{mtr,\, historical} = \beta_t + \varepsilon_{mt} + \gamma_{mtr} \quad \text{(eq. 2.2)}$$

where the total signal of $x_{mtr,\, historical}$ is split into three different terms: the multi-model mean time evolution of the externally forced signal (β_t), the deviation of the externally forced response of model m from the multi-model externally forced response (ε_{mt}), and the evolution of the internal variability (γ_{mtr}).

To focus on the divergence among models of the temporal variability, we remove to each *historical* simulation the common β_t signal, and we refer to those residuals as detrended *historical* simulations, which we call *historical_DT*. The conceptual statistical decomposition of *historical_DT* is:

$$x_{mtr,\, historical\_DT} = \varepsilon_{mt} + \gamma_{mtr} \quad \text{(eq. 2.3)}$$

From eqs. (2.3), we can decompose the temporal variance of the *historical_DT* simulations into:

$$\sigma_t^2(x_{mr})_{historical\_DT} = \sigma_t^2(\varepsilon_m) + \sigma_t^2(\gamma_{mr}) + 2cov_t(\varepsilon_m, \gamma_{mr}) \quad \text{(eq. 2.4)}$$

where the notation σ_t^2 indicates the variance is computed over the time dimension and $cov_t(u, v)$ represents the temporal covariance between two variables u and v such as: $cov_t(u, v) = \frac{1}{(T-1)} \sum_{t=1}^{T} u_t v_t$.

A-c) Quantifying the relative contributions of the externally driven and internally driven variability

To separate variations of x_{mtr} between variations driven by the model specific response to external forcing (ε_{mt}) and the variations driven by internal variability (γ_{mtr}), one would need several realizations of historical simulations per model. However, in this study we only consider one realization per model ($R = 1$). Therefore, $x_{mtr} = x_{mt}$, $\gamma_{mtr} = \gamma_{mt}$ and the terms ε_{mt} and γ_{mt} cannot be disentangled. Eqs. 2.3 and 2.4 become:

$$x_{mt,\, historical\_DT} = \varepsilon_{mt} + \gamma_{mt} \quad \text{(eq. 2.5)}$$

$$\sigma_t^2(x_m)_{historical\_DT} = \sigma_t^2(\varepsilon_m) + \sigma_t^2(\gamma_m) + 2cov_t(\varepsilon_m, \gamma_m) \quad \text{(eq. 2.6)}$$

This implies that we cannot decompose the temporal variance of x_{mt} into an externally forced component and an internally driven component using *historical_DT* only.

To gain insight on the role played by internal variability (γ) on the variance of x, we analyze the *piControl* simulations. In those simulations the external forcings are kept constant and by construction the time variability can only arise from internal variability. The conceptual statistical decomposition of *piControl* is:

$$x_{mt,\,piControl} = \gamma_{mtr} \quad \text{(eq. 2.7)}$$

And its temporal variance is simply:

$$\sigma_t^2(x_{mr})_{piControl} = \sigma_t^2(\gamma_{mr}) \quad \text{(eq. 2.8)}$$

From Eqs. 2.6 and 2.8, we can estimate the multi-model average ($\overline{\sigma_t^2(x)}$) and the inter-model variance ($\sigma_m^2\left[\sigma_t^2(x)\right]$) of the temporal variance from the *historical_DT* and *piControl* datasets.

Case of the *historical_DT* simulations:

$$\overline{\sigma_t^2(x)_{historical\_DT}} = \overline{\sigma_t^2(\varepsilon)} + \overline{\sigma_t^2(\gamma)} + \overline{2cov_t(\varepsilon,\gamma)} \quad \text{(eq. 2.9)}$$

$$\sigma_m^2\left[\sigma_t^2(x)\right]_{historical\_DT} = \sigma_m^2\left[\sigma_t^2(\varepsilon)\right] + \sigma_m^2\left[\sigma_t^2(\gamma)\right] + \sigma_m^2\left[2cov_t(\varepsilon,\gamma)\right]$$
$$+\ 2cov_m\left[\sigma_t^2(\varepsilon), \sigma_t^2(\gamma)\right] +\ 2cov_m\left[\sigma_t^2(\varepsilon), 2cov_t(\varepsilon,\gamma)\right] +\ 2cov_m\left[\sigma_t^2(\gamma), 2cov_t(\varepsilon,\gamma)\right] \quad \text{(eq. 2.10)}$$

where the overbar in Eq. 2.9 indicates the average among models and where σ_m^2 in Eq. 2.10 indicates the variance is computed along the model dimension: $\sigma_m^2\left[\sigma_t^2(x)\right] = \frac{1}{(M-1)}\sum_{m=1}^{M}\left(\sigma_t^2(x_m) - \overline{\sigma_t^2(x_m)}\right)^2$

Case of the *piControl* simulations:

$$\overline{\sigma_t^2(x)_{piControl}} = \overline{\sigma_t^2(\gamma)} \quad \text{(eq. 2.11)}$$

$$\sigma_m^2\left[\sigma_t^2(x)\right]_{piControl} = \sigma_m^2\left[\sigma_t^2(\gamma)\right] \quad \text{(eq. 2.12)}$$

Comparing the inter-model variance of the *historical_DT* (eq. 2.9) and of the piControl (eq. 2.12), we can quantify the proportion of the variance coming from internal variability in *hisotrical_DT* and therefore the origin of the inter-model variance in those simulations.

Section 3: Variance analysis of eq. 1

Taking into account that the atmospheric growth rate can be written as:

$$\frac{dCO2}{dt} = CO2_{Emissions} + CO2_{Ocean} + CO2_{Land} \ (eq.\,3.1\,)$$

The variance of $\frac{dCO2}{dt}$ can be expressed as:

$$\sigma^2\left(\frac{dCO2}{dt}\right) = \sigma^2(CO2_{Emissions}) + \sigma^2(CO2_{Ocean}) + \sigma^2(CO2_{Land}) + 2cov(CO2_{Emissions}, CO2_{Ocean}) + + 2cov(CO2_{Emissions}, CO2_{Land}) + 2cov(CO2_{Ocean}, CO2_{Land}) \quad (eq.\ 3.2)$$

Table 3.1 shows the percentage of the total variance of $\frac{dCO2}{dt}$ which is explained by each one of the terms in eq. 3.2.

Product\Variance ratio	**var($CO2_{Land}$)**	**var($CO2_{Ocean}$)**	**var($CO2_{Emissions}$)**	**2*cov($CO2_{Land}$,$CO2_{Ocean}$)**	**2*cov($CO2_{Ocean}$, $CO2_{Emissions}$)**	**2*cov($CO2_{Lann}$, $CO2_{Emissions}$)**
CSIR	92,00	8,79	98,96	12,98	-55,62	-57,11
Zeng	95,53	5,75	98,96	12,5	-41,98	-70,75
Iida	117,06	2,28	98,96	-5,56	1,07	-113,81
Watson	99,78	7,14	98,96	6,86	-39,59	-73,15
GraCER	99,17	4,02	98,96	10,58	-34,47	-78,27
CMEMS	99,52	3,5	98,96	10,76	-33,16	-79,57
Landschuetzer	94,85	8,45	98,96	10,48	-47,34	-65,4
Roedenbeck	97,12	10,21	98,96	6,45	-45,30	-67,43
Multimodel mean	99.38	6.26	98.96	8.13	-37.05	-75.69

Table 3.1. Percentage of $\sigma^2\left(\frac{dCO2}{dt}\right)$ which is explained by each one of the terms in the variance analysis (eq. 3.2).

Section 4: Quantifying the uncertainty in total CO2 fluxes in observations

Figure 4.1(a) shows the evolution of the atmospheric CO2 concentration rate without the externally forced signal (green line). Focusing on this curve, results show the existence of two different periods before and after 1960. Before 1960, the variability of the atmospheric CO2 concentration showed larger amplitude than after 1960. Focusing on the period after 1960 and in order to quantify the uncertainty of the variability in the atmospheric CO2 concentration rate due to the shortness of the observational period, we computed the standard deviation of the atmospheric CO2 concentration rate considering different moving windows in the period 1960-2014 with the same length that the original observed (28 years: 1986-2013). Results can be observed on Figure 4.1(b) where it is possible to see that depending on the moving window one chooses, the variability of the fluxes changes. In addition, we can observe values encompassed by the multi-mode spread in the historical CMIP6 simulations (compare Figure 4.1 with Figure 1 in the manuscript).

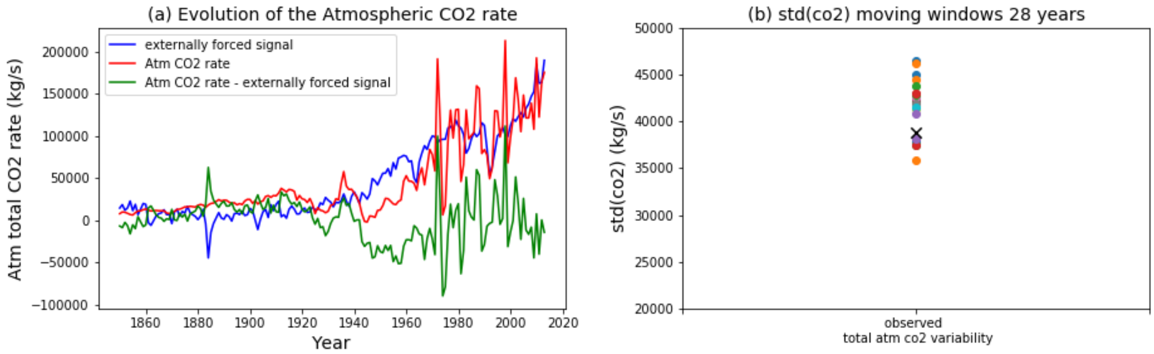

Figure 4.1. (a) Evolution of the atmospheric CO2 concentration rate from 1850 to 2014 without removing the externally forced signal (red) and removing it (green). Blue curve represents the externally forced signal computed as the multimodal mean of all the models in Table 1 plus emissions. (b) standard deviation of the atmospheric CO2 considering different moving windows of 28 years length from 1960 to 2013.

Section 5. Variance analysis of $CO2_{Land}$

The global air-land CO2 fluxes ($CO2_{Land}$) can be written as follow:

$$CO2_{Land} = \sum_{i=1}^{4} CO2_{Land-i} + R \quad \text{(eq. 5.1)}$$

where $CO2_{Land-i}$ represents the air-land CO2 fluxes over each one of the key regions in Figure 3a (Amazonian, South Tropical Africa, Southeast Asia and Oceania) plus a residue. Therefore, the temporal variance of $CO2_{Land}$ can be expressed as:

$$\sigma_t^2(CO2_{Land}) = \sum_{i=1}^{4} \sigma_t^2(CO2_{Land-i}) + 2\sum_{i\neq j} cov(CO2_{Land-i}, var(CO2_{Land-j}) + 2\sum_{i=1}^{4} var(CO2_{Land-i}, R)$$
(eq. 5.2)

Table 5.1 shows the percentage of the $\sigma_t^2(CO2_{Land})$ which is explained by each one of the key regions and the covariance terms. Results on this table are related to the multi-model mean.

Region	% of $\sigma^2(CO2_{Land})$ explained
Amazonian	22
South Tropical Africa	10
South east Asia	5
Oceania	4
Residue	25

$2\sum_{i\neq j} cov(CO2_{Land-i}, var(CO2_{Land-j})$	23
$2\sum_{i=1}^{4} var(CO2_{Land-i}, R)$	11

Table 5.1. Percentage of the $\sigma^2(CO2_{Land})$ which is explained by each one of the key regions and the covariance terms. Results on this table are related to the multi-model mean.

Section 6. Decomposition of the global $\sigma^2_{t,Land}$ into its regional contribution

The global air-land CO2 fluxes ($CO2_{Land}$) can be written as follow:

$$CO2_{Land} = CO2_{Land-Tropics} + CO2_{Land-Extratropics} \quad \text{(eq. 6.1)}$$

where $CO2_{Land-Tropics}$ represents the air-land CO2 fluxes over all the key regions in Figure 3a (Amazonian, South Tropical Africa, Southeast Asia and Oceania) and $CO2_{Land-Extratropics}$ the total air-land CO2 for the rest of the world. Therefore, the temporal variance of $CO2_{Land}$ can be expressed as:

$$\sigma^2_t(CO2_{Land}) = \sigma^2_t(CO2_{Land-Tropics}) + \sigma^2_t(CO2_{Land-Extratropics}) + 2\sum_{i\neq j} cov(CO2_{Land-Tropics}, CO2_{Land-Extratropics})$$
(eq. 6.2)

Then, the variance across models:

$$\sigma^2\left[\sigma^2_t(CO2_{Land})\right] = \sigma^2\left[\sigma^2_t(CO2_{Land-Tropics})\right] + \sigma^2\left[\sigma^2_t(CO2_{Land-Extratropics})\right] +$$

$$+ \sigma^2\left[2cov(\sigma^2_t(CO2_{Land-Tropics}, CO2_{Land-Extratropics})\right] + 2cov\left[\sigma^2_t(CO2_{Land-Tropics}), \sigma^2_t(CO2_{Land-Extratropics})\right] +$$

$$+ 2cov\left[\sigma^2_t(CO2_{Land-Tropics}), 2cov[CO2_{Land-Tropics}, CO2_{Land-Extratropics}]\right] +$$

$$+ 2cov\left[\sigma^2_t(CO2_{Land-Extratropics}), 2cov[CO2_{Land-Tropics}, CO2_{Land-Extratropics}]\right] \quad \text{(eq. 6.3)}$$

The residual term computed for Figure 4 represents the addition of $2cov\left[\sigma^2_t(CO2_{Land-Tropics}), 2cov[CO2_{Land-Tropics}, CO2_{Land-Extratropics}]\right]+$

$2cov\left[\sigma_t^2(CO2_{Land-Extratropics}), 2cov[CO2_{Land-Tropics}, CO2_{Land-Extratropics}]\right]$, denoted as cov2 and cov3 terms, respectively, on Figure 4 caption.

Section 7. Correlation maps in CMIP6 models

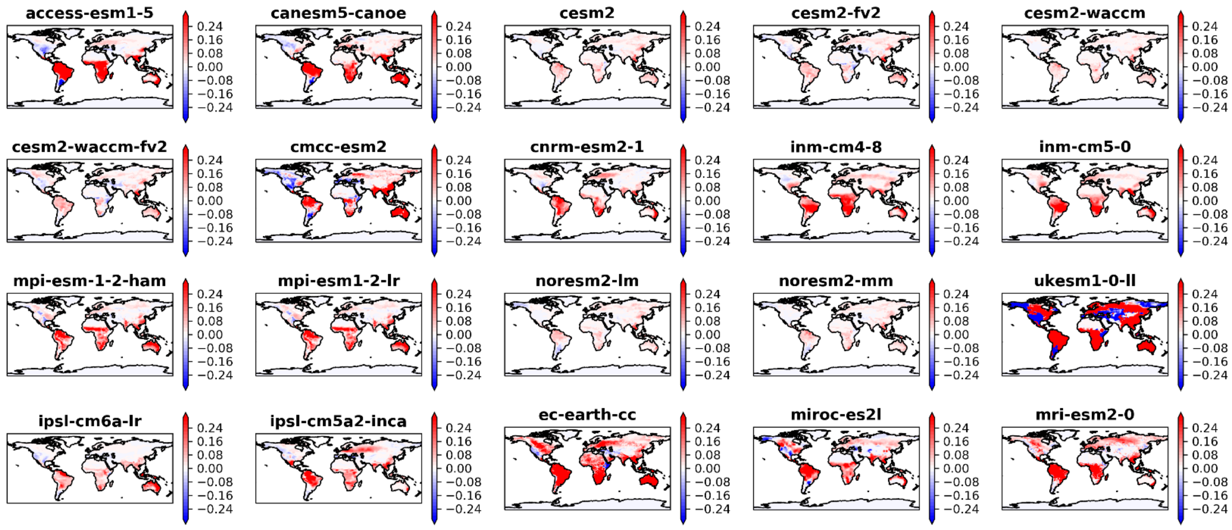

Figure 7.1. Regression maps between the global $CO2_{Land}$ fluxes and the local $CO2_{Land}$ fluxes. Annual means from Jan to Dec.

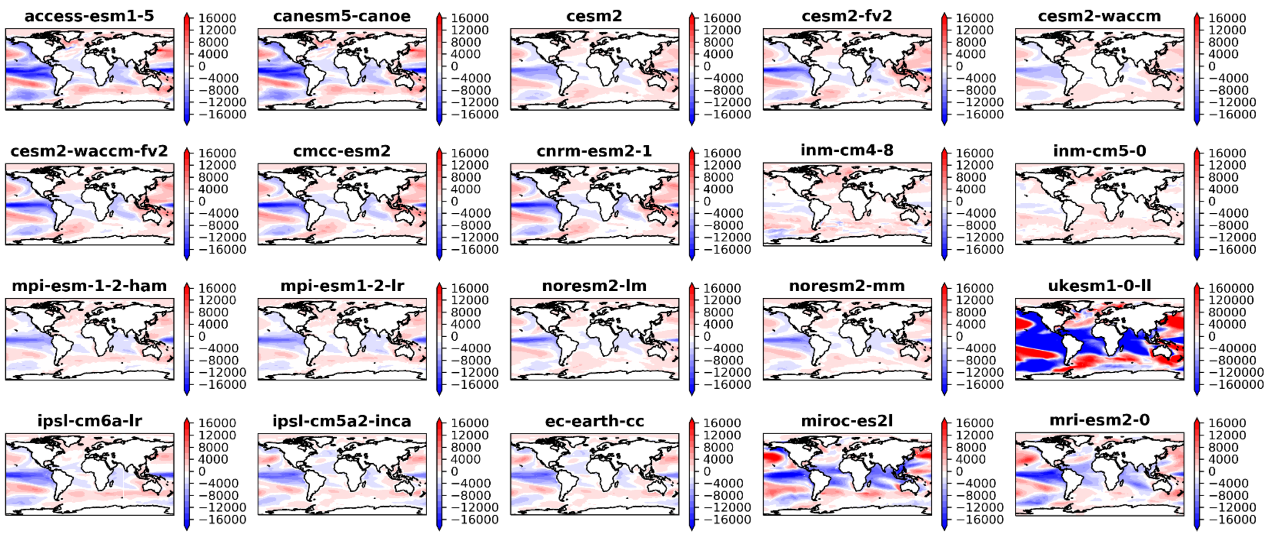

Figure 7.2. Regression maps between the global $CO2_{Land}$ fluxes and the SST anomalies. Annual means from Jan to Dec.

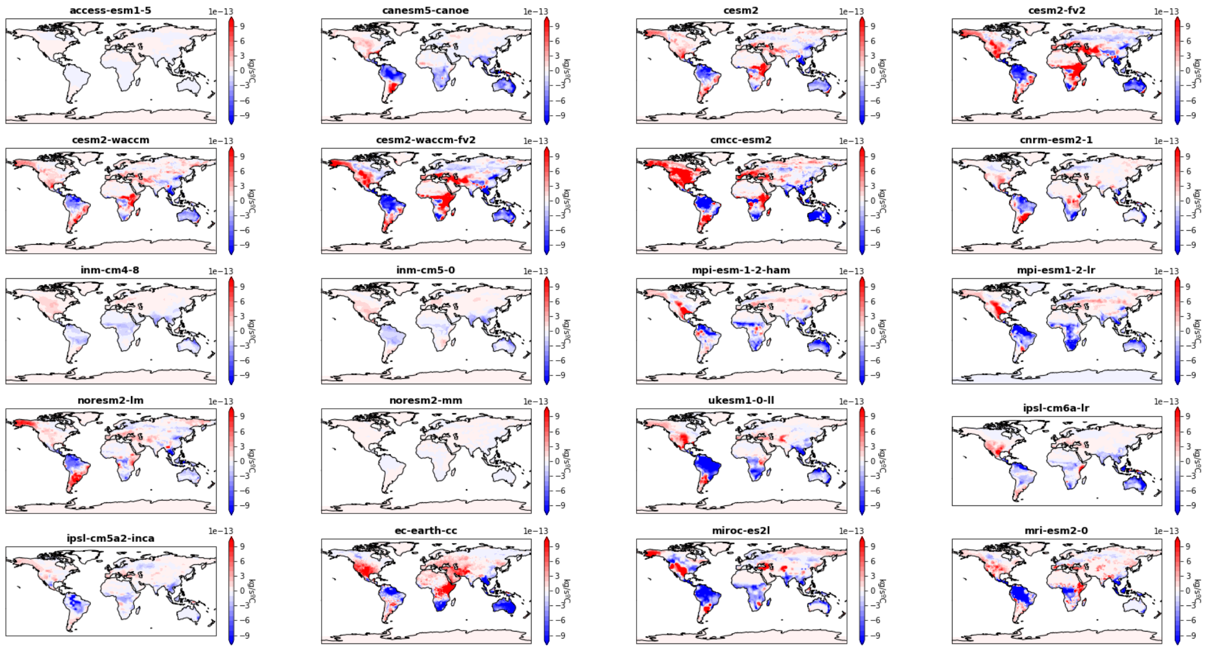

Figure 7.3. Correlation map between nino4 and the local $CO2_{Land}$ fluxes. Nino4 centered on Oct to March and CO2 fluxes on Jan to Dec of the following year.

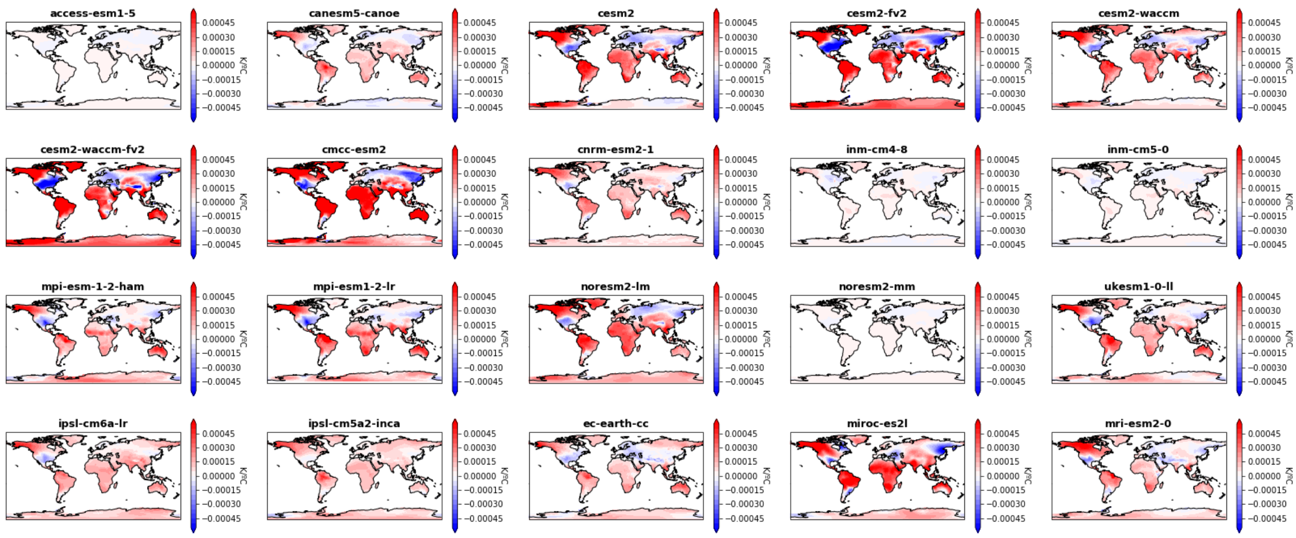

Figure 7.4. Regression maps between Niño4 and TAS. Nino4 centered on Oct to March and TAS is the annual mean from Jan to Dec.

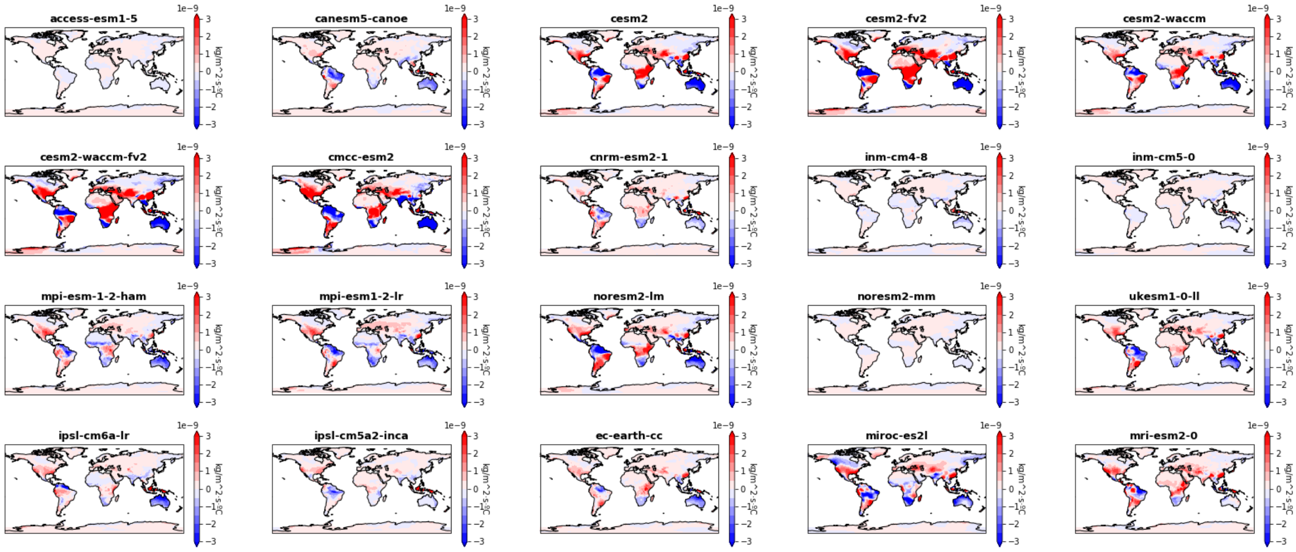

Figure 7.5. Correlation map between the nino4 index centered in Oct to March and the precipitation anomalies annual mean from Jan to Dec.

Section 8. Scatter plots sensitivities

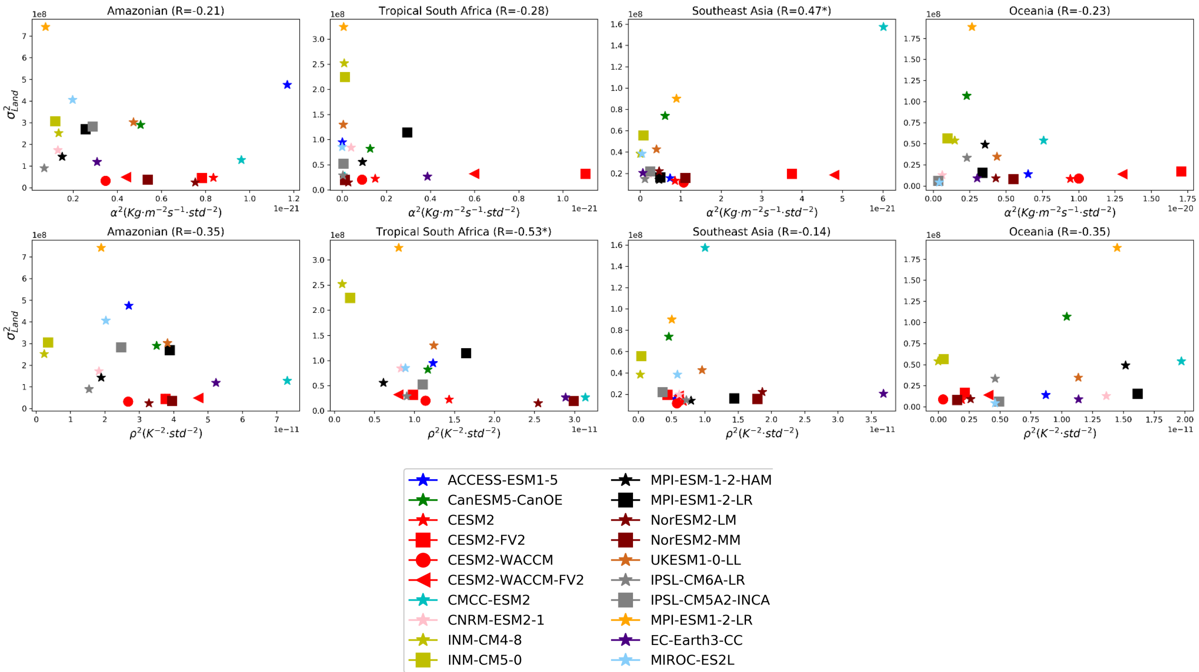

Figure 8.1. Scatterplots of the $\sigma^2_{t,Land}$ over each key region (in Fig 3a) vs. square of the sensitivity of precipitation (α^2, first row) or surface air temperature (ρ^2, second row) to Nino4 normalized in the same key region. Key regions are the Amazonian (first column), Tropical South Africa (second column), Southeast Asia (third column) and Oceania (fourth column). The area that represents each one of the regions is marked on Figure 3a. Values with an * exceed 95% level of confidence from one-tailed t-test.

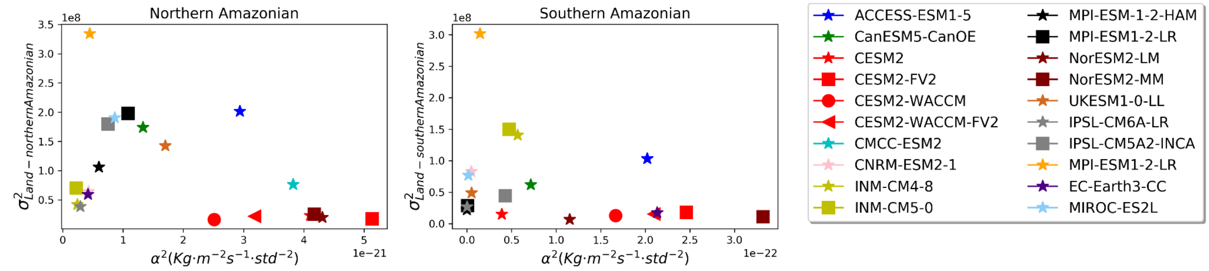

Figure 8.2. Scatterplots of the $\sigma^2_{t,Land}$ vs. square of the sensitivity of precipitation (α^2) to Nino4 normalized over the northern and southern Amazonian region. The Northern Amazonian covers [280ºE-320ºE,10ºN-10ºS] and the southern one [280ºE-320ºE,10ºS-30ºS]. Correlations are -0.43 for the northern part and -0.30 for the southern one). None of them are statistically significant considering 95% level of confidence from one-tailed t-test.